Technologies and Materials for Renewable Energy, Environment & Sustainability

Enhancing Mixing Performance of Inline Mixers Under Laminar Flow Conditions

Enhancing Mixing Performance of Inline Mixers Under Laminar Flow Conditions

Mosbah Kiwan[1, a)], Cathy Castelain [1, b)], and Teodor Burghelea[1, c)]

[1] *Nantes Université, CNRS, Laboratoire de thermique et énergie de Nantes, LTeN, UMR6607, F-44000 Nantes, France*

[a)] *Corresponding author: mosbah.kiwan@etu.univ-nantes.fr*
[b)] *cathy.castelain@univ-nantes.fr*
[c)] *teodor.burghelea@univ-nantes.fr*

Abstract. Efficient mixing of viscous Newtonian fluids remains a critical challenge in the development of compact and sustainable process systems. This study examines experimentally laminar chaotic mixing in an inline mixer using laser-induced fluorescence (LIF) to characterize scalar transport. Instantaneous fluorescence images are processed into spacetime diagrams, which capture the evolution of concentration fields along the flow direction across time. From these diagrams, we extract the rate of concentration fluctuations as a quantitative measure of local mixing intensity. By systematically varying the mixing protocol, we construct spatial maps of mixing efficiency across a range of operating conditions. The results reveal clear trends in mixing performance as a function of flow parameters and offer quantitative benchmarks for mixer optimization. This work provides new insights into scalar transport in viscous laminar flows and supports the energy-efficient design of continuous mixing systems for sustainable processing applications.

INTRODUCTION

The efficient mixing of viscous fluids remains a critical challenge in many industrial processes, including cosmetics, food production, and chemical manufacturing [1, 2]. In such systems, mixing through molecular diffusion is often too slow due to the high viscosity, making the process inefficient and energy-intensive [3]. One approach to accelerate mixing is through turbulence, which enhances the interfacial area and reduces mixing time. However, for highly viscous fluids, generating turbulence requires significant energy input and introduces high shear stresses that may degrade sensitive materials [4].

An alternative, energy-efficient strategy for enhancing mixing in laminar regimes is chaotic advection, which induces complex fluid trajectories without requiring turbulence. This mechanism generates exponential stretching and folding of fluid interfaces, significantly increasing mixing efficiency under low Reynolds number conditions [2, 5, 6,7]. First conceptualized by Aref [6] and further formalized by Ottino [2], chaotic advection arises when flow symmetries are broken through spatial or temporal perturbations [8]. Passive strategies, such as staggered herringbone grooves [9], serpentine channels [10], or helical static mixers [11], rely on geometric features to induce secondary flows and streamline deformation. In contrast, active methods introduce time-dependent disturbances, including oscillatory flows [12], electro kinetic instabilities [13], or acoustic and mechanical vibrations [14, 15], to further enhance mixing performance.

To harness the benefits of chaotic advection in a continuous-flow system while minimizing energy input and shear-related damage, this study investigates an active inline chaotic mixer. Originally introduced by El Omari et al. [16], the mixer comprises three rotating cylinders embedded near the walls of a straight mixing channel. The mixing is confined to a relatively short segment of the total channel length, and the rotating elements generate controlled secondary flows that induce repetitive stretching and folding of fluid elements. While prior research has focused on theoretical modeling and numerical simulations [16], this work extends the investigation through a detailed experimental study of mixing performance in viscous Newtonian fluids. This is done using laser-induced fluorescence to examine the change in the mixing efficiency with respect to the operating protocols. This study provides new insights into the dynamics of mixing under varying operational conditions, thereby contributing to the design of sustainable and energy-efficient continuous mixers for industrial applications.

EXPERIMENTAL SETUP

Experimental Bench

The rotating arc wall mixer (RAW) consists of a channel with width W=2 cm, height H=4 cm, and total length L=20 cm; schematic drawings are presented in Fig. 1a and Fig. 1b. It consists of three main zones (see Fig. 2a), first the converging zone with an angle 45°. The entering fluids are separated by a fin to postpone the interaction between the fluids until the mixing zone. Next, there is the mixing zone where the fluid enters with an average speed U to the zone where the external perturbation occurs, and thus the mixing, and, finally, the exit zone. In the mixing zone, three rotating cylinders of radius R=1cm, made of the same transparent material, are positioned vertically along with the channel height and inserted inside the mixing channel with a protrusion distance Δ= 0.33 cm. The cylinders located on the same side of the wall are separated by a distance d=3 cm. Each rotating cylinder is connected to a separate stepping motor (National Instruments, ST24-E model) and can operate independently. The exit channel is set to 8 cm to reduce the backflow effects of the exit port into the mixing zone and give the possibility to measure, independent of the measurements in the mixing zone, the mixing properties at the exit of the mixing process.
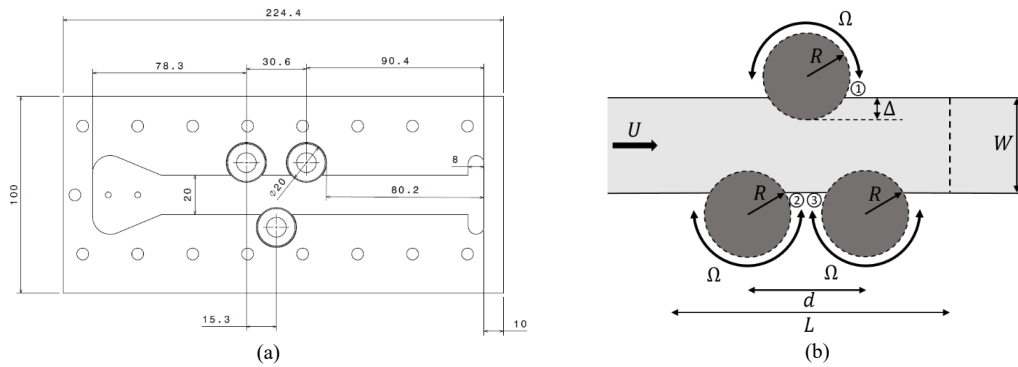

(a)   (b)

FIGURE 1. (a) Dimension drawing of the mixer, (b) Schematic drawing of the mixer

The generation of chaotic trajectories inside the mixing channel is obtained by alternating the rotation of the cylinder in the mixing zone. The rotation of those cylinders is governed by the following protocol:

$$\Omega = \Omega_0 \sin(2\pi f t + \phi) \tag{1}$$

where Ω_0, f, and Ω are the rotational speed amplitude, the alternating frequency, and the phase shift, respectively. The cylinder located opposite to the cylinders located on the same side is phase-shifted by 1π. All three cylinders rotate at the same alternating frequency and amplitude. Also, the choice of this rotational protocol is based on the findings published by El Omari et al. [16] where modulating the perturbation of the flow with a sine function (introducing the time variable) and with opposite directions of rotation generates chaotic flow topologies. Such flow structures are formed by the alternating perturbation in the flow, thus creating elliptical regions and a hyperbolic point in the center of the flow in the mixing zone. Visualizing such points and alternating between the formation and destruction favors higher occurrences of stretching and folding of fluid elements and thus better mixing. The system is then controlled by both the amplitude and frequency of rotation. These two parameters are the ones that define the efficiency of this operating mixer, for which two non-dimensional parameters could be defined:

$$K = \frac{R\Omega_0}{U} \tag{2}$$

$$St = \frac{Wf}{U} \tag{3}$$

where K and St are the speed ratio and Strouhal number, respectively. K is defined as the ratio between the rotational velocity of the perturbing cylinders and the bulk flow velocity, while St is defined as the ratio between the flow characteristic time and the perturbation period.

The supply system feeding into the mixer consists of two syringes made in-house, each housing approximately 4.5 liters of fluid. They are fabricated using the same transparent material as that used with the mixer and ensure a

continuous fluid supply at a defined and precise flow rate while withstanding the high pressure formed inside. Each cylinder operates separately by a high-precision linear actuator (Thomson Linear Motion, Model PC32LX999B04-0400FM1) that pushes through a shaft inside the syringe, a head made of polyoxymethylene plastic with two O-ring seals to prevent leakage and fluid loss from the active side of the cylinder (see Fig. 2b). The control of all the moving parts within the experimental bench is done with a LabVIEW interface.
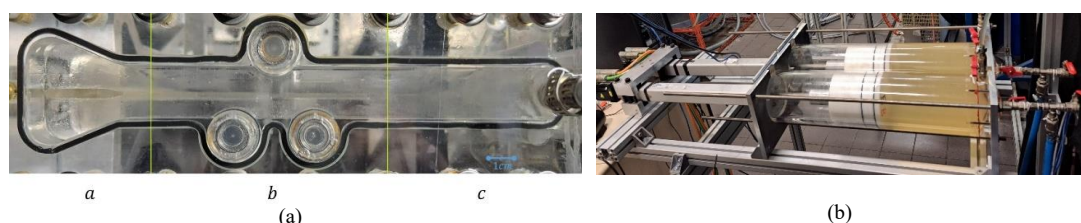

FIGURE 2. (a) Mixer's zones: a. Converging, b. Mixing, and c. Exit (b) Supply cylinders

The optical alignment is the key component for the experimental campaigns. It is designed to illuminate the center plane of the channel along the main direction of flow. For this distribution, a 532 nm continuous steady-state 3W laser (LD PUMPED ALL-SOLID-STATE GREEN LASER by Changchun New Industries Optoelectronics Tech) has been used whose output beam is deflected, split into two, and directed into laser line generator lenses (75° Full Fan Angle Laser Line Generator Lens by Edmund Optics) from the side where there is only one cylinder. Although the cylinder is made of the same transparent material as the mixer, it acts as an obstacle and creates shadows inside the channel due to the difference in the refractive index. Therefore, the laser beam is split into two and oriented in two directions to compensate for the dark zone in the shadows. The camera used for visualizing the flow is a 12-bit monochrome camera from Basler (Basler ace-acA1920-155um) with a spatial resolution of 1920 pixels by 1200 pixels set at 156 frames per second and mounted with a 35 mm lens from Edmond Optics mounted on the camera, obtaining a pixel length of 38 μm.

Tested fluid

Emkarox^{TM} HV45 is an industrial name for polyoxyalkylene glycol, commonly used as a water-soluble polymer. It is supplied by Croda (France) and has a unique, faint yellowish color. It is characterized by its high viscosity (100 Pa.s in its non-diluted form), allowing a wide range of viscosities when diluted at different concentrations with a density of around 1090 kg.m^{-3} at 20°C. EMKAROX is often used in industrial applications such as lubrication, viscosity modification, and as a thickener in hydraulic fluids. Its Newtonian behavior makes it a useful reference fluid for studying flow and mixing processes in different applications. For further information, refer to https://msds.crodadirect.com/ using the product code: ETK0694. This fluid is diluted to a concentration of 50% by weight to acquire a dynamic viscosity of 1.7 Pa.s. The reason why this fluid has been used in this study is the range of viscosities that it gives. The chosen viscosity of 1.7 Pa·s ensures that, at a flow rate of 20 Lph, the flow operates at a Reynolds number of Re=0.1. The accuracy of the bulk flow velocity estimation was verified using both classical volumetric flow measurements and particle image velocimetry (PIV), the latter employed in a separate study. Across the range of operating conditions, the relative error remained low, with an average value not exceeding 5.88%.

EXPERIMENTAL TECHNIQUES

To understand the relying phenomena in the mixer and the mixing process, laser-induced fluorescence (LIF) experiments were performed. LIF experiments allow direct measurement of the degree of mixing. The flow is divided into two, the first using fluorescein dye and the second without any additive dye. The mixing zone is illuminated as described in the previous section; in this case, the fluid with the dye emits bright light, while the one without dye does not. The concentration of dye added to the fluid is 0.0032% by weight. The laser power is set to its maximum power (3 watts), and the exposure time of the camera is 6ms. This configuration of the camera parameters and concentration of fluorescein dye gives access to all 4096 grey levels of the 12-bit camera used. Although mixing patterns are observed within the mixing zone between the cylinders, the mixing degree index is measured near the channel outlet to avoid accounting for fluid elements still undergoing the mixing process. Measurements are preferably taken at a

location where the flow is fully developed and the concentration gradients have stabilized, ensuring a representative assessment of the final mixing state.

DATA PROCESSING

To understand the mixing phenomenon and identify the efficient mixing protocol, this study relies on measuring the concentration field standard deviation analysis (C_{std}).
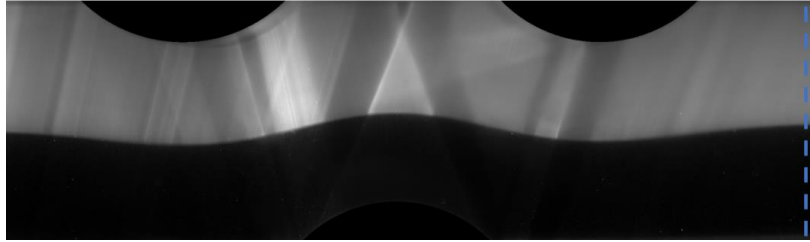

FIGURE 3. Mixing zone

Evaluating the mixing intensity is done by calculating the standard deviation of the concentration field around the exit of the mixing channel. Accordingly, a line profile is extracted at the beginning of the outlet section (dotted blue line in Fig. 3) to evaluate the degree of homogeneity in a controlled and meaningful manner. It is a classical method in which you can identify how homogeneous the mixture is at the end of the process. Consider where two fluids are set to mix; the thinner the superposed fluid filaments at the exit, the better the mixing is considered. Thus, lower values of these fluctuations hint at better mixing. Images acquired from the LIF experiment are passed through a proper normalizing algorithm, where the presence of the dye yields 1, 0 where there is no dye, and 0.5 indicates ideal mixing. The normalizing is done at the beginning of each experiment to reduce any effect of condition changes by the following:

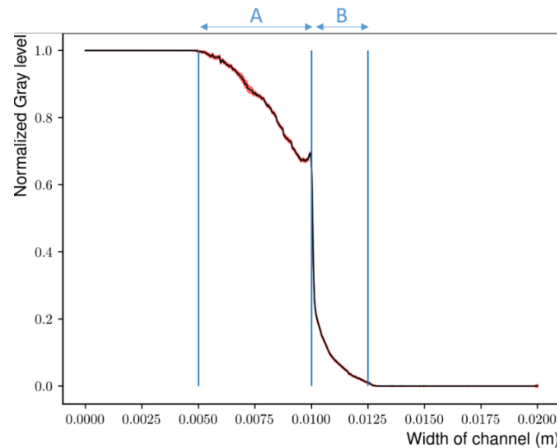$$C = \frac{C_0 - C_{\min}}{(C_0 - C_{\min})_{\max}} \tag{4}$$

FIGURE 4. Normalized gray level distribution across the width of the channel for the case with no rotation

Fig. 4 presents the grey level intensity distribution across the width of the channel. As the excitation light traverses the fluorescent fluid, its intensity gradually diminishes due to both scattering and attenuation associated with increasing optical path length. Upon reaching the interface between the fluorescent and non-fluorescent regions, denoted as Zone A in Fig. 4, a marked drop in signal is observed, transitioning sharply from the bright to the dark region. This transition is followed by a subtle rise in intensity in Zone B, attributed to light reflected or scattered from

adjacent illuminated areas. Ideally, the resulting fluorescence intensity profile should exhibit two plateaus at either end, representing the fully fluorescent and non-fluorescent regions, respectively, separated by a sharp, nearly vertical transition corresponding to the interface. All following results are calibrated based on the given distribution presented in Fig. 4. Following the normalization process, a space-time diagram is constructed at the specified region around the exit in Fig. 3 to visualize the temporal evolution of the concentration distribution, whose standard deviation could be calculated as:

$$C_{std} = \sqrt{\frac{1}{n}\sum_{i=1}^{n}(C-\overline{C})^2} \tag{5}$$

RESULTS

Identifying the optimal mixing protocol for this type of fluid involves direct visualization of a mixing experiment, allowing for qualitative and quantitative assessment of the evolving concentration fields. By observing the extent of homogenization, interface deformation, and persistence of unmixed zones, one can evaluate the actual mixing performance and validate the effectiveness of the chosen protocol. In this visualization, the white regions correspond to fluid volumes that have been mixed with the fluorescent dye, while the black regions represent the fluid without any dye. This qualitative experiment aims to illustrate the extent of homogeneity achieved under the specified flow protocol. While the visualization provides useful insight into the general mixing pattern at the observed location, it is inherently qualitative.
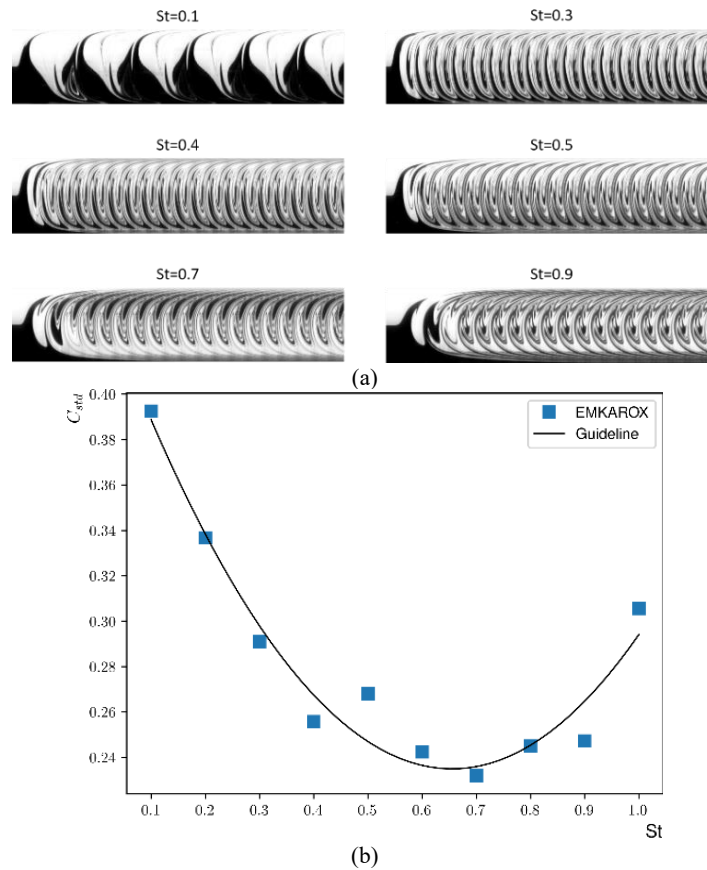

(a)

(b)

FIGURE 5. (a) Representation of Space-time diagrams at different Strouhal numbers, (b) A complete comparison of the C_{std} mean value for K=10

Since the quantitative analysis is confined to a specific line section at the channel exit, a more comprehensive representation of mixing dynamics can be achieved by constructing a space-time diagram. This is done by stacking the spatial profiles of this line section across the entire temporal domain of data acquisition. The resulting diagram, some examples of which are presented in Fig. 5a, offers a valuable visualization of the scalar field evolution. Through this approach, one can readily observe whether the scalar is undergoing effective stretching and folding or if large, unmixed fluid regions persist, indicating poor homogenization. As time progresses and higher-order periods are reached, the space-time diagrams show that the flow tends to converge toward a stable, periodic trend that repeats consistently, indicating a quasi-steady mixing regime. The total number of periods captured varies depending on the Strouhal number, ranging from approximately 7.5 periods for St=0.1 up to 75 periods for St=1. Applying the C_{std} approach to the acquired space-time diagrams enables the evaluation of the temporal evolution of the mixing efficiency measure. The corresponding mixing efficiencies, derived from the average of the final five periods, are presented in Fig. 5b. This plot reveals a non-monotonic relationship between the Strouhal number and mixing performance. Notably, the measure reaches its minimum at St=0.7, indicating optimal mixing conditions at this frequency.
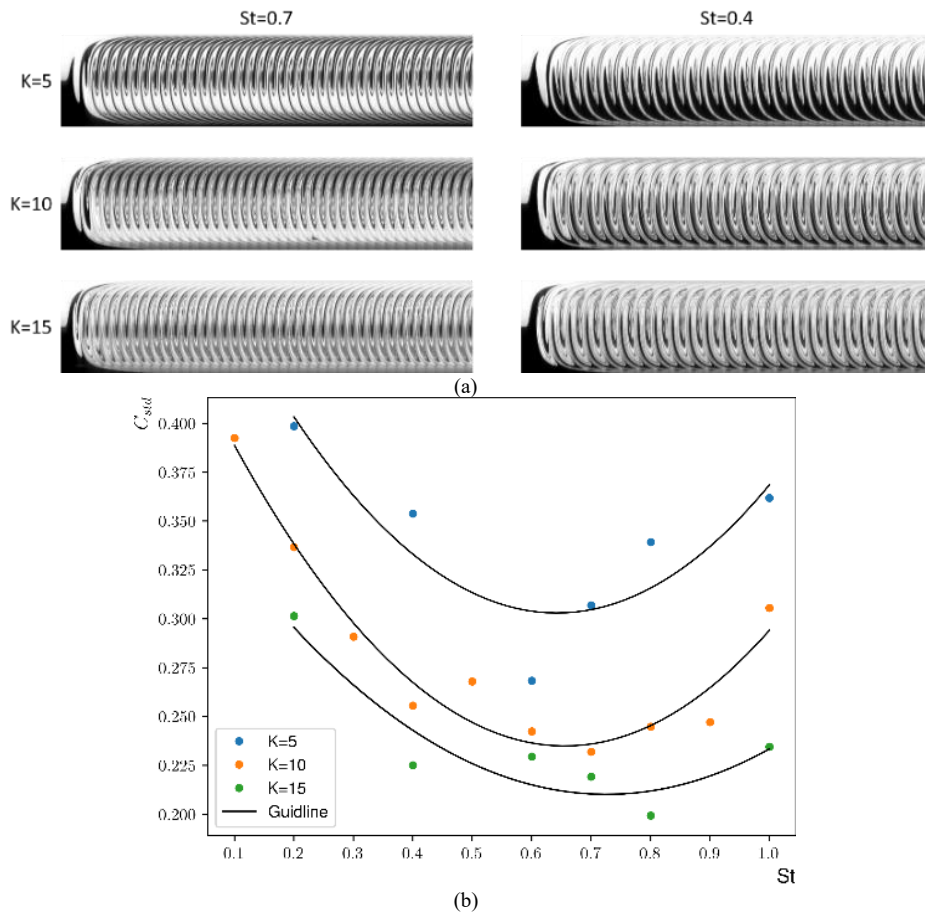

FIGURE 6. (a) Representation of Space-time diagrams for two Strouhal numbers at different K values (K=5, K=10, and K=15), (b) A complete comparison of the C_{std} mean value for three different K values (K=5, K=10, and K=15)

After identifying an optimal Strouhal number that enhances mixing performance, the focus is now shifted toward investigating the influence of the forcing amplitude, represented by the parameter K, on the mixing efficiency. This analysis aims to establish a consistent framework for evaluating a performance map of the mixer when operating with a Newtonian fluid. Fig. 6a presents space-time diagrams for two selected Strouhal numbers, St=0.7 and St=0.4, under three different values of K. Qualitatively, an increase in K appears to promote greater homogenization of the scalar field. To quantitatively assess this trend, the mixing efficiency measure C_{std} was computed across the different cases.

The results indicate that a decrease in the perturbation amplitude (i.e., lower K) corresponds to diminished mixing efficiency, while higher values of K lead to enhanced mixing performance; see Fig. 6b. Moreover, these results are in good agreement with the findings reported by El Omari et al [16]. The trends observed across different Strouhal numbers exhibit consistent and self-similar behavior with respect to variations in K, with the location of the minimum shifting depending on the value of K.

CONCLUSION

This study experimentally investigated the mixing performance of the RAW mixer using a Newtonian fluid, with mixing efficiency quantified through scalar concentration fields obtained via Laser-Induced Fluorescence (LIF) measurements. The analysis revealed the existence of an optimal mixing condition at a Strouhal number St=0.7 for a speed ratio K=10, where homogenization is maximized. Furthermore, variations in the speed ratio K significantly influenced mixing efficiency: increasing K enhanced the mixing, while decreasing it reduced efficiency. Additionally, the location of the minimum concentration fluctuations shifted systematically with changes in K. These findings provide valuable insights for optimizing operating parameters in continuous mixing processes. These findings provide valuable insights for optimizing operating parameters in continuous mixing processes and contribute to the development of compact, energy-efficient, and sustainable mixing systems suited for modern industrial applications. It also paves the way to understand future approaches to the use of fluids with non-Newtonian behavior. Further investigations will focus on understanding the influence of non-Newtonian rheology on the mixing process, with particular attention to how shear-thinning behavior and yield stress alter flow structures and mixing efficiency.

ACKNOWLEDGMENTS

REFERENCES

1. V. A. Atiemo-Obeng, S. M. Kresta, and E. L. Paul, *Handbook of Industrial Mixing: Science and Practice* (Wiley-Interscience, Hoboken, 2004).
2. J. M. Ottino, *The Kinematics of Mixing: Stretching, Chaos, and Transport* (Cambridge University Press, Cambridge, 1989).
3. N.-T. Nguyen and Z. Wu, *J. Micromech. Microeng.* **15**, R1 (2004).
4. F. Raynal and J.-N. Gence, *Int. J. Heat Mass Transf.* **40**, 3267 (1997).
5 F. J. Muzzio, P. D. Swanson, and J. M. Ottino, *Phys. Fluids A* **3**, 822 (1991).
6. H. Aref, *J. Fluid Mech.* **143**, 1 (1984).
7. H. Aref *et al.*, *Rev. Mod. Phys.* **89**, 025007 (2017).
8. S. Wiggins and J. M. Ottino, *Philos. Trans. R. Soc. A* **362**, 937 (2004).
9. A. D. Stroock *et al.*, *Science* **295**, 647 (2002).
10. C.-H. Lee, C.-H. Lin, and Y.-H. Lin, *J. Micromech. Microeng.* **16**, 1649 (2006).
11. Kenics Corporation, U.S. Patent 3,042,247 (1960).
12. G. Metcalfe, M. Rudman, A. Brydon, L. J. W. Graham, and R. Hamilton, *AIChE J.* **52**, 9 (2006).
13. M. H. Oddy, J. G. Santiago, and J. C. Mikkelsen, *Anal. Chem.* **73**, 5822 (2001).
14. Y. Liu, J. Liu, W. Chen, and S. Shi, *IEEE Trans. Ultrason. Ferroelectr. Freq. Control* **59**, 981 (2012).
15. N.-T. Nguyen and Z. Wu, *J. Micromech. Microeng.* **15**, R1 (2005).
16. K. El Omari *et al.*, *Phys. Rev. Fluids* **6**, 024502 (2021).